

# Flow of CO<sub>2</sub>–ethanol and of CO<sub>2</sub>–methanol in a non-adiabatic microfluidic T-junction at high pressures

R. Blanch-Ojea · R. M. Tiggelaar · J. Pallares ·  
F. X. Grau · J. G. E. Gardeniers

Received: 18 August 2011 / Accepted: 4 November 2011 / Published online: 18 January 2012  
© Springer-Verlag 2012

**Abstract** In this work, an experimental investigation of the single- and multiphase flows of two sets of fluids, CO<sub>2</sub>–ethanol and CO<sub>2</sub>–methanol, in a non-adiabatic microfluidic T-junction is presented. The operating conditions ranged from 7 to 18 MPa, and from 294 to 474 K. The feed mass fraction of CO<sub>2</sub> in the mixtures was 0.95 and 0.87, respectively. Under these operating conditions, CO<sub>2</sub> was either in liquid, gas or supercritical state; and the mixtures experienced a miscible single phase or a vapour–liquid equilibrium (VLE), with two separated phases. Taylor, annular and wavy were the two-phase flow regimes obtained in the VLE region. In the single phase region, the observed flows were classified into standard single-phase flows, “pseudo” two-phase flows and local phenomena in the T-junction. Flow regime maps were generated, based on temperature and pressure conditions. Two-phase flow void fractions and several parameters of Taylor flow were analysed. They showed a clear dependency on temperature, but were mostly insensitive to pressure. A continuous accumulation of liquid, either in the CO<sub>2</sub> channel or at the CO<sub>2</sub>-side wall after the T-junction, disturbed most of the experiments in VLE conditions by randomly generating liquid plugs. This phenomenon is analysed, and capillary

and wetting effects due to local Marangoni stresses are suggested as possible causes.

**Keywords** Microchannels · T-junction · Two-phase flows · Vapour–liquid equilibrium · Supercritical carbon dioxide

## List of symbols

|             |                                                         |
|-------------|---------------------------------------------------------|
| $C$         | Correlation parameter (–)                               |
| $G_d$       | Vaporized mass diffusion fraction (–)                   |
| $N$         | Number of liquid plugs (–)                              |
| $P$         | Pressure (MPa)                                          |
| $R$         | Pixel resolution of images (pixel m <sup>-1</sup> )     |
| $T$         | Temperature (K)                                         |
| $\% v/v$    | Volumetric fraction (–)                                 |
| $\Delta px$ | Difference in pixel position between two frames (pixel) |
| $d_h$       | Hydraulic diameter of the channel (m)                   |
| $f$         | Frequency (Hz)                                          |
| $fr$        | Camera frame rate (Hz)                                  |
| $t$         | Time (s)                                                |
| $u$         | Velocity (m s <sup>-1</sup> )                           |
| $x$         | Mass fraction in liquid phase (–)                       |
| $x_o$       | Mass fraction in mixture (–)                            |
| $y$         | Mass fraction in vapour phase (–)                       |

**Electronic supplementary material** The online version of this article (doi:10.1007/s10404-011-0927-x) contains supplementary material, which is available to authorized users.

R. Blanch-Ojea (✉) · J. Pallares · F. X. Grau  
Department of Mechanical Engineering, Rovira i Virgili  
University, Campus Sescelades, 43007 Tarragona, Spain  
e-mail: roland.blanch@urv.cat

R. M. Tiggelaar · J. G. E. Gardeniers  
Mesoscale Chemical Systems, MESA+ Institute for  
Nanotechnology, University of Twente, P.O. Box 217,  
7500 AE Enschede, The Netherlands

## Greek symbols

|               |                               |
|---------------|-------------------------------|
| $\rho$        | Density (kg m <sup>-3</sup> ) |
| $\theta$      | Elongation rate (–)           |
| $\varepsilon$ | Void fraction (–)             |

## Subscripts

|     |              |
|-----|--------------|
| bn  | Bubble nose  |
| bub | Bubble point |
| bt  | Bubble tail  |
| dew | Dew point    |
| exp | Experimental |

|     |                         |
|-----|-------------------------|
| hom | Homogeneous             |
| l   | Liquid phase            |
| lp  | Liquid plug             |
| o   | Syringe pump conditions |
| rel | Relative                |
| v   | Vapour phase            |
| xio | Xiong and Chung (2007)  |

### Abbreviations

|                 |                           |
|-----------------|---------------------------|
| CO <sub>2</sub> | Carbon dioxide            |
| EtOH            | Ethanol                   |
| MeOH            | Methanol                  |
| VLE             | Vapour–liquid equilibrium |

## 1 Introduction

Provided that gas–liquid and liquid–liquid multiphase flows, in both adiabatic and non-adiabatic microchannels, have been proven to differ to their veteran macroscopic counterparts (Kandlikar 2002; Thome 2006; Shao et al. 2009), the study of these microfluidic systems has become nowadays a topic of great interest and, therefore, extensive information can be found in recent publications.

In their series of reviews, Shui and her co-workers (Shui et al. 2007a, b) addressed the different phenomena, the actuation and manipulation methods and the applications of multiphase flows of immiscible fluids in micro- and nanochannels. Their reviewed applications included emulsification, encapsulation, microreaction, chemical synthesis, mixing, bioassay, biological enzymatic degradation, extraction, separation and kinetic studies. The available experimental data dealing with adiabatic gas–liquid flows in microchannels, the existing flow regimes, the influence of different parameters in their transitions and the broad range of flow regime maps previously presented in literature were included in the reviews of Akbar et al. (2003) and Shao et al. (2009). Kandlikar (2002) and Thome (2006) focused their overviews on flow boiling in single- and multi-microchannels. They summarised the existing two-phase flow regimes, their corresponding maps and the flow prediction methods, they also discussed about critical heat fluxes, flow instabilities and pressure drops. In their review of the physics behind microfluidics, Squires and Quake (2005) devoted a section to the existing phenomena and available techniques for manipulating and controlling solid–liquid and multiphase fluid systems. Guido and Preziosi (2010) presented a review on experimental and numerical literature concerning the physics of droplet flow behaviour in microchannels, such as deformation and breakup, and the effect of surfactants on the aforementioned behaviour.

Although most of the work on multiphase flow in microchannels so far has been devoted either to boiling

flows of single fluids in non-adiabatic conditions (e.g. Revellin et al. 2006; Agostini et al. 2008; Revellin et al. 2008), or to flows of immiscible fluids in adiabatic conditions, with each fluid present exclusively in one of the phases (e.g. Kawahara et al. 2002; Chung and Kawaji 2004; Guillot and Colin 2005; Garstecki et al. 2006; de Loos et al. 2010), the use of potentially miscible fluids is also feasible. A two-phase flow of two potentially miscible fluids can be achieved if the mixture, originally in a miscible single phase, is taken to certain temperature and pressure conditions where its thermodynamic phase equilibrium, also known as vapour–liquid equilibrium (VLE), occurs (Smith et al. 2000). In VLE, the mixture splits into two coexisting, separated, immiscible liquid and vapour phases. However, unlike the usual flows of immiscible fluids in adiabatic conditions, here there is a mass transport of each fluid to both immiscible phases, in a proportion specific to the temperature and pressure conditions.

Two-phase flow systems of fluids experiencing VLE can be applied to generate fluid micromixers or microreactors. These benefit from the control of the composition of liquid and vapour phases by selecting the appropriate temperature and/or pressure conditions. The possibility to manipulate the surface tension forces, which are important in the dynamics of flows in microfluidic channels, is another interesting feature. On the other hand, the unique properties of supercritical fluids, i.e. their easily tunable physical properties, their high diffusivity and their zero surface tension, make them very attractive for a number of applications not only at macro- but also at micro- and nano-scales (Chehroudi 2006). CO<sub>2</sub> has gained special attention among these supercritical fluids. It is cheap, non-flammable, non-toxic, environmentally friendly, with a moderate critical point (7.37 MPa and 304.2 K), and it is advantageous in a broad range of applications such as extraction processes, cooling in microchannels (e.g. Cheng et al. 2008), or as reaction solvent in microreactors (e.g. Trachsel et al. 2009).

Few related studies with fluids experiencing VLE (e.g. Hwang et al. 2005; Weinmueller et al. 2009) or with supercritical fluids (e.g. Dang et al. 2008; Marre et al. 2009) are available in the two-phase flow literature. However, at the studied experimental conditions their equilibrium compositions are as in the usual immiscible fluids without mass transport between phases, with each phase composed exclusively by a single fluid.

Motivated by this situation, the aim of the present work is to study experimentally the single and multiphase flow of two sets of potentially miscible fluids, CO<sub>2</sub>–ethanol (CO<sub>2</sub>–EtOH) and CO<sub>2</sub>–methanol (CO<sub>2</sub>–MeOH), over a non-adiabatic microfluidic T-junction, in order to gain understanding on the behaviour of these systems at different conditions of temperature and pressure. Within such

range of conditions the alcohols were in liquid state, the CO<sub>2</sub> was either in liquid, gas or supercritical state, and their mixtures covered the single phase and the VLE regions.

## 2 Experimental

### 2.1 Microfluidic chip layout

A microfluidic chip made of Borofloat glass (width ( $W$ )  $\times$  length ( $L$ )  $\times$  height ( $H$ ) = 15  $\times$  20  $\times$  2 mm) was used in this work. Figure 1 shows a layout of the chip. The cross-sectional geometry of the main channels is semicircular ( $W_{mc} \times H_{mc} = 70 \times 30 \mu\text{m}$ ;  $d_h = 39.3 \mu\text{m}$ ). The microfluidic resistor ( $W_{fr} \times H_{fr} = 20 \times 5 \mu\text{m}$ ) maintains constant the upwards pressure in the meandering channel of the chip. Fused silica capillaries with standard polyimide coating (Polymicro Technologies TSP040105) were glued (Araldite Rapid) to the inlets and outlet of the chip for withstanding high operating pressures. Further details of the design, fabrication and testing of the microfluidic chip can be found elsewhere (Tiggelaar et al. 2007).

As shown in Fig. 1, two areas ( $W' \times L' = 8.2 \times 7.4 \text{ mm}$ ) were cooled and heated by placing on top of the glass chip, respectively, a thermoelectric Peltier element (Melcor CP0.8-7-06) glued to a copper block, and an electric resistor on top of a second copper block. Heat sink silicone compound (Dow Corning 340) was used for improving contact. The cooled area nearby the inlets kept both fluids in liquid state at temperatures around 283–288 K as they entered the chip. The heated area, on the other hand, included the T-junction and the area visualised with the microscope ( $W'' \times L'' = 0.325 \times 0.696 \text{ mm}$ ).

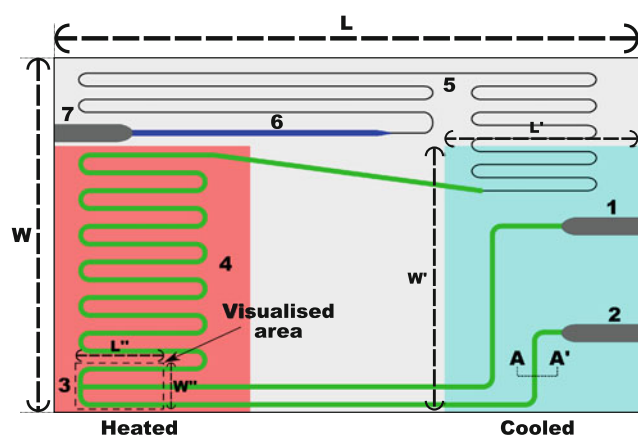


**Fig. 1** Layout of the glass microfluidic chip. Legend: 1 Alcohol inlet; 2 CO<sub>2</sub> inlet; 3 T-junction; 4 meandering channel; 5 fluidic resistor; 6 expansion zone; 7 outlet. The area visualised with the microscope during the experiments, as well as the heated and cooled areas, is indicated. Dimensions:  $W = 15 \text{ mm}$ ;  $L = 20 \text{ mm}$ ;  $W' = 8.2 \text{ mm}$ ;  $L' = 7.4 \text{ mm}$ ;  $W'' = 0.325 \text{ mm}$ ;  $L'' = 0.696 \text{ mm}$

The heated copper block ensured that both fluids reach the T-junction already at the experimental temperature and state.

### 2.2 Experimental setup

A sketch and a brief description of the experimental setup used in this work have been included in Online Resource 1.

### 2.3 Operating conditions

The system pressure ranged from 7 to 18 MPa, and it was set and monitored by means of the syringe pump. Although the fluidic resistor (see Fig. 1) minimised the pressure losses within the chip channels, a slight pressure drop of around 3 % from the pump to the T-junction was estimated, comparing present experimental results of saturation pressures of CO<sub>2</sub> with theoretical data.

The experimental temperature of the copper block on top of the glass chip was measured with a Pt100 sensor (with values that ranged from 294 to 500 K), whereas the temperature of the bottom of the glass chip was measured with an auxiliary sensor. In this way, the effective temperature in the T-junction was estimated by calculating the vertical temperature gradient across the chip, at different temperatures of the copper block.

The feed ratio of fluids could not be monitored or controlled during the experiments. This ratio was estimated by comparing present experimental visualisations of the bubble point of the mixtures at different pressures, with available experimental literature data of VLE. For doing so, a chip similar to the one shown in Fig. 1, but with the T-junction placed in the cooled area instead, was used. In this case, the fluids are mixed prior to reach the heated area and, depending on the temperature, they experience a phase separation. The procedure allowed to accurately estimate the mass fractions in the mixtures,  $x_{o,CO_2} \approx 0.95$  ( $\%v/v_{o,CO_2} \approx 0.949$ ) for CO<sub>2</sub>–EtOH and  $x_{o,CO_2} \approx 0.87$  ( $\%v/v_{o,CO_2} \approx 0.869$ ) for CO<sub>2</sub>–MeOH. Unlike previous works, here the feed ratio of fluids was constant throughout the study, whereas the composition of the separated vapour and liquid phases during VLE, as well as the vaporisation of the mixture, varied depending on temperature and pressure conditions.

The total feed flow rate was monitored with the flow meter included in the syringe pump (but it could not be controlled, due to pressure-mode operation of the pump). Nevertheless, a continuous oscillation in the readings during the experiments due to the operation mode of the pump precluded an accurate monitoring and, therefore, only approximate values could be estimated, from  $\sim 3 \mu\text{l min}^{-1}$  at 7 MPa to  $\sim 7 \mu\text{l min}^{-1}$  at 10 MPa and to  $\sim 13 \mu\text{l min}^{-1}$  at 18 MPa.

**Table 1** Approximate linear velocities of the fluids reaching the T-junction

| Fluid                           | P/MPa | T/K | $u/\text{m s}^{-1}$ |
|---------------------------------|-------|-----|---------------------|
| CO <sub>2</sub> (liquid)        | 7     | 294 | 0.027               |
|                                 | 18    | 294 | 0.11                |
| CO <sub>2</sub> (gas)           | 7     | 314 | 0.11                |
|                                 | 7     | 474 | 0.26                |
| CO <sub>2</sub> (supercritical) | 8     | 314 | 0.13                |
|                                 | 18    | 474 | 0.48                |
| EtOH                            | 7     | 294 | 0.0015              |
|                                 | 18    | 474 | 0.0095              |
| MeOH                            | 7     | 294 | 0.0038              |
|                                 | 18    | 474 | 0.025               |

Based on the feed ratio of fluids and the estimated total feed flow rate from the syringe pump, the linear velocities of the fluids reaching the T-junction could be approximately calculated by means of mass and volumetric flow balances between the syringe pump and the T-junction. Due to its different states, the CO<sub>2</sub> experienced the most widespread range of velocities, although these were very similar in the two different mixtures. Table 1 includes the approximated velocities of the fluids. At these velocities and experimental conditions, the values of Reynolds number based on  $d_h$  ranged from  $\approx 10$  to  $\approx 150$  for the CO<sub>2</sub>, while they did not exceed  $\approx 5$  for the EtOH and MeOH. It is worth remarking, on one hand, that these velocity and Reynolds values must only be considered as approximated and, on the other hand, that these velocities do not correspond to the usual superficial velocities defined in the literature.

#### 2.4 Image analysis

During each experiment, 50–450 images were recorded with a CCD high-speed camera (PCO 1200s) attached to an inverted microscope (LEICA DMI5000M), at exposure times of 20–30  $\mu\text{s}$  and maximum frame rates,  $fr$ , of 940 Hz, with a size of  $541 \times 1,160$  pixels per frame. The pixel resolution of the images,  $R$ , was  $0.600 \text{ pixel } \mu\text{m}^{-1}$ . Each stack of images was processed with “ImageJ Image Processing Software” (Rasband 1997–2011) for the two-phase flows analysis.

The void fraction of the experiments,  $\varepsilon_{\text{exp}}$ , and the liquid–vapour interfaces were determined and identified, respectively, in a similar way to the one of Agostini et al. (2008). When calculating the void fraction, the thin liquid layers on top and bottom of the channel were neglected. The non-uniform distribution of the area-to-volume fraction associated with the cross-sectional geometry of the channel was not taken into account.

Once the images were already processed, the velocity of liquid plugs,  $u_{\text{lp}}$ , was determined as,

$$u_{\text{lp}} = 0.5 \cdot (u_{\text{bt}} + u_{\text{bn}}) \quad (1)$$

Both the bubble tail and nose velocities,  $u_{\text{bt}}$  and  $u_{\text{bn}}$ , were calculated as,

$$u = \frac{fr \Delta px}{R} \quad (2)$$

where  $\Delta px$  is the difference in pixel position of the liquid–vapour interface among two successive frames.

The elongation rate,  $\theta$ , measured by means of the ratio of elongation of a plug to the distance it travelled along the channel, was defined as,

$$\theta = \frac{u_{\text{bt}} - u_{\text{bn}}}{u_{\text{lp}}} \quad (3)$$

Finally, the frequency of liquid plugs during a video sequence was determined as,

$$f_{\text{lp}} = \frac{N - 1}{\Delta t} \quad (4)$$

where  $N$  is the number of plugs and  $\Delta t$  is the elapsed time between the first and the last liquid plug observed in the video sequence.

### 3 Results and discussion

#### 3.1 Phase behaviour of mixtures

Both CO<sub>2</sub>–EtOH and CO<sub>2</sub>–MeOH belong to the so-called Type I binary mixtures. These mixtures are characterised by their complete miscibility in liquid state and their simplest fluid phase behaviour, experiencing VLE always at temperatures between the saturation lines of both fluids, i.e. with one fluid in liquid state and the other in gas or supercritical state (Chester 2004). In VLE, the mass fraction of fluids in both immiscible phases,  $x$  and  $y$ , is determined by the temperature and pressure conditions. Outside this VLE region only single phase can exist, either in liquid–liquid, vapour–vapour or supercritical–liquid form (Smith et al. 2000).

P-T-x-y data of VLE for both sets of fluids were obtained from several authors (Secuianu et al. 2008; Joung et al. 2001; Jennings et al. 1991; Suzuki et al. 1990; Galicia-Luna et al. 2000; Brunner et al. 1987; Ohgaki and Katayama 1976; Bezanhtak et al. 2002; Leu et al. 1991; Mendoza de la Cruz and Galicia-Luna 1999; Tian et al. 2001). These data allowed the estimation of the mass composition of the working mixtures (see Sect. 2.3), and further identification of the VLE boundaries at these compositions in the P-T based maps of single and two-phase flow regimes (see Sect. 3.2).

The phase behaviour for both mixtures at three different pressures, 6.89, 7.87 and 9.81 MPa, is shown in Fig. 2, with the CO<sub>2</sub> mass fractions in the the mixture, and in the liquid and vapour phases. The VLE regions, the bubble and dew point lines, and several tie lines are indicated. A steep gradient in  $x_{CO_2}$  can be seen for all VLE cases at temperatures close to the bubble point, which gradually decreases as temperature approaches the dew point. This variation in  $x_{CO_2}$  can lead to important changes in the properties of the liquid phase in equilibrium, as well as in the vaporisation of the mixture and in the flow conditions. On the other hand,  $y_{CO_2}$  remains relatively constant at all VLE temperatures, especially in the case of CO<sub>2</sub>–EtOH mixture.

### 3.2 Flow regimes

Two independent scenarios were identified for the study of flow behaviour of the two sets of fluids, CO<sub>2</sub>–EtOH and CO<sub>2</sub>–MeOH, over a T-junction. The first, at the operating conditions under which the mixture experienced VLE and

two-phase flows occurred, with both phases separated by an interface with a finite interfacial tension; and the second, with single-phase mixtures and single-phase flows.

Unlike previous literature, in the present work the liquid alcohols, a.k.a. continuous phase, were fed from the side channel of the T-junction, whereas the gas CO<sub>2</sub> or supercritical CO<sub>2</sub>, a.k.a. disperse phase, were fed from the main channel of the T-junction (Fig. 1). The centrifugal forces generated in the curvature of the channel after the T-junction did not affect the observed flow regimes and, therefore, the associated Dean effects can be considered negligible.

In the two-phase flows scenario three pressures were tested, 6.89, 7.87 and 9.81 MPa. According to the definitions from Shao et al. (2009), Revellin (2005) and Lee and Lee (2008), Taylor and annular were the main observed two-phase flow regimes for both mixtures in VLE conditions. The flow regimes are shown in Fig. 3 for CO<sub>2</sub>–MeOH. Wavy flow was also observed under certain conditions, whereas bubbly, churn, dispersed or rivulet flows did not appear. No different regimes other than those already reported in gas–liquid systems were found in the experiments with supercritical CO<sub>2</sub>.

Figure 4 shows the maps of two-phase flow regimes inside the VLE regions based on temperature and the three pressures tested. The saturation line of CO<sub>2</sub> and the boundaries of VLE regions of CO<sub>2</sub>–EtOH at  $x_{o,CO_2} = 0.95$  and CO<sub>2</sub>–MeOH at  $x_{o,CO_2} = 0.87$  are included in the maps for completeness. In both cases, annular flow was obtained

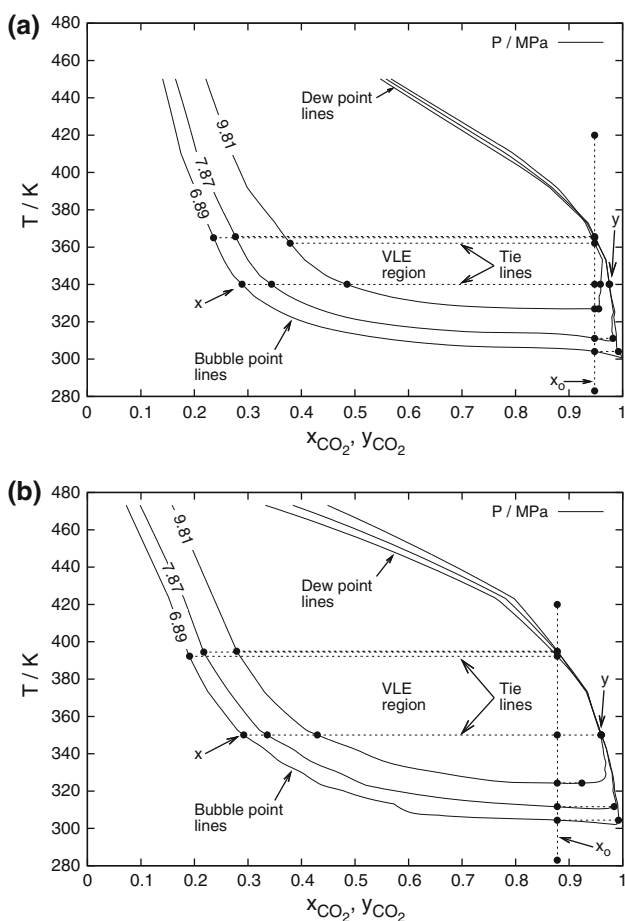


**Fig. 2** T-x-y diagrams from literature data for mixtures of **a** CO<sub>2</sub>–EtOH and **b** CO<sub>2</sub>–MeOH, at different pressures: 6.89, 7.87 and 9.81 MPa. The phase behaviour for the mixtures at **a**  $x_{o,CO_2} = 0.95$  and **b**  $x_{o,CO_2} = 0.87$  is indicated

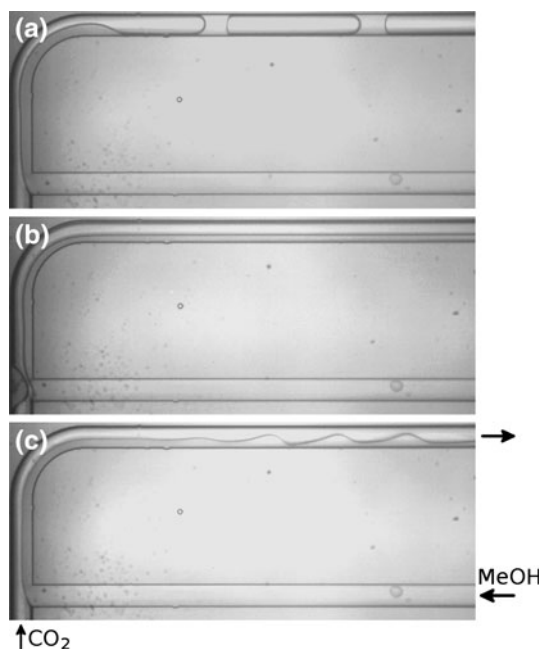


**Fig. 3** Two-phase flow regimes of CO<sub>2</sub>–MeOH mixture: **a** Taylor ( $P = 7.87$  MPa,  $T = 310.4$  K); **b** Annular ( $P = 9.81$  MPa,  $T = 331.4$  K); **c** Wavy ( $P = 9.81$  MPa,  $T = 323.4$  K)



almost throughout the entire regions analysed, in particular, for CO<sub>2</sub>–EtOH. Taylor flow was typical of lower pressures and low–medium temperatures, being more common in the CO<sub>2</sub>–MeOH system where it was obtained at 6.89 and 7.87 MPa. The predominance of annular flow is usually favoured by significant inertial forces and by high gas-to-liquid rates (Shao et al. 2009). This is consistent with the very high vaporised fractions obtained in the present work in most of the experimental conditions (see Sect. 3.4). It also agrees with the high contents of CO<sub>2</sub> in the liquid phases (Fig. 2) which decrease the interface tension. The increased velocities of the vapour phase, a result of increased feed rates at higher pressures and temperatures, also support the predominance of annular flows. Taylor flow is more common for CO<sub>2</sub>–MeOH than for CO<sub>2</sub>–EtOH, which is probably due to lower vaporised fractions shown

in the first mixture. The effect of different fluid properties should be minor because the large content of CO<sub>2</sub> in both liquid phases should balance their properties. Note that methanol is less viscous and it has higher surface tension than ethanol. Wavy flow was obtained in a few occasions, always nearby the bubble point limits of the VLE regions at the highest pressure tested. The failure to maintain the wavy flow over a wider range of temperatures might be due to the sharp gradients of the CO<sub>2</sub> content in liquid phases (Fig. 2) and of the vaporised fractions in these regions, as it will be discussed in Sect. 3.4.

It can be seen in Figs. 5 and 6 that a series of flow regimes were observed outside the VLE region, including the expected standard single-phase flows as well as a variety of “pseudo” two-phase flows and two local phenomena in the T-junction. Examples of the listed regimes and phenomena can be observed in Fig. 5 for CO<sub>2</sub>–MeOH, and the corresponding regime maps for CO<sub>2</sub>–EtOH and CO<sub>2</sub>–MeOH based on temperature and pressure conditions are included in Fig. 6.

The standard single-phase flows were mostly found at low temperature, in the form of either liquid CO<sub>2</sub>–liquid alcohol (Fig. 5a) or supercritical CO<sub>2</sub>–liquid alcohol (Fig. 5b). Characteristic of these flows was a mixing layer after the T-junction, without a clearly recognisable interface between both fluids.

At certain pressure and temperature conditions, the mixing layer turned into a clear interface between both phases, resulting in a “pseudo” two-phase flow along the mixing distance after the T-junction, just to disappear as both fluids reached a homogeneous mixing and became single-phase flow. The downstream extension of the “pseudo” two-phase flows, measured from the T-junction, always increased with pressure. The flow regimes in the “pseudo” two-phase flow were stratified (smooth) (Fig. 5c, d), Taylor (Fig. 5e) and wavy (Fig. 5i). The main observed regime was “pseudo” stratified flow which, especially at higher pressures and at temperatures above the VLE region, decreased its extension as temperature increased (Fig. 5c, d). In fact, the VLE regions were surrounded by this “pseudo” stratified flow, with the exception of a small region between the saturation line of CO<sub>2</sub> and the bubble point line, of around 2–3 K, where “pseudo” Taylor flow was observed. The extension of the “pseudo” Taylor flow increased as temperature approached the bubble point of the mixture.

The “pseudo” wavy flow and the two local phenomena, namely meniscus and boiling, were only observed at higher temperatures. For both phenomena, the liquid alcohol was quickly absorbed by the CO<sub>2</sub> stream in the T-junction, and therefore no liquid flow reached the main channel (Fig. 5f, g). Meniscus (Fig. 5f) was observed at lower pressures, both below and above supercritical CO<sub>2</sub> conditions, and

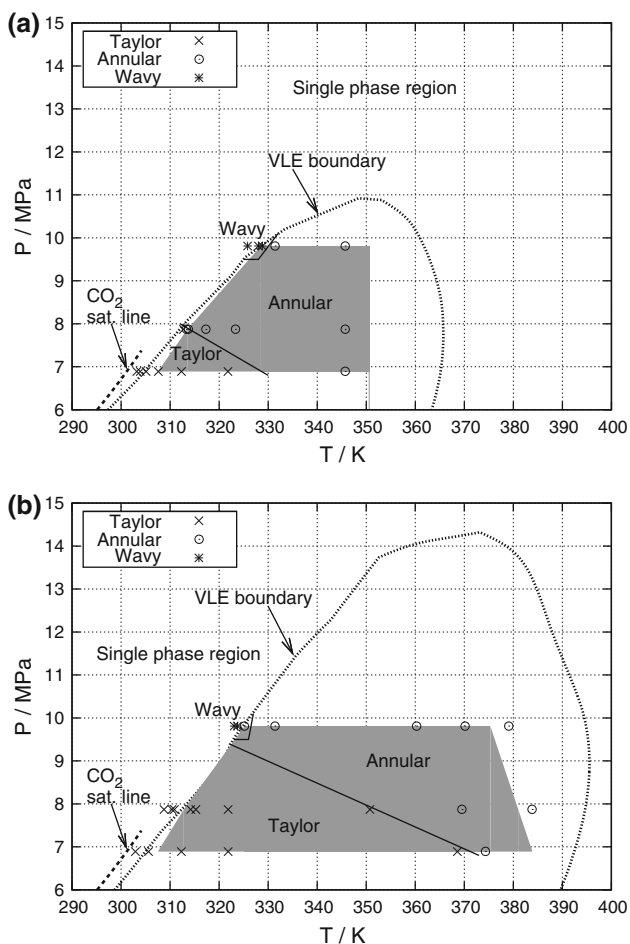


**Fig. 4** Maps of two-phase flow regimes for mixtures of **a** CO<sub>2</sub>–EtOH and **b** CO<sub>2</sub>–MeOH, based on temperature and pressure conditions. The boundaries of VLE regions at **a**  $x_{0,CO_2} = 0.95$  and **b**  $x_{0,CO_2} = 0.87$  are indicated. The shaded areas correspond to the experimental conditions where the liquid accumulation phenomenon was observed (see Sect. 3.3)

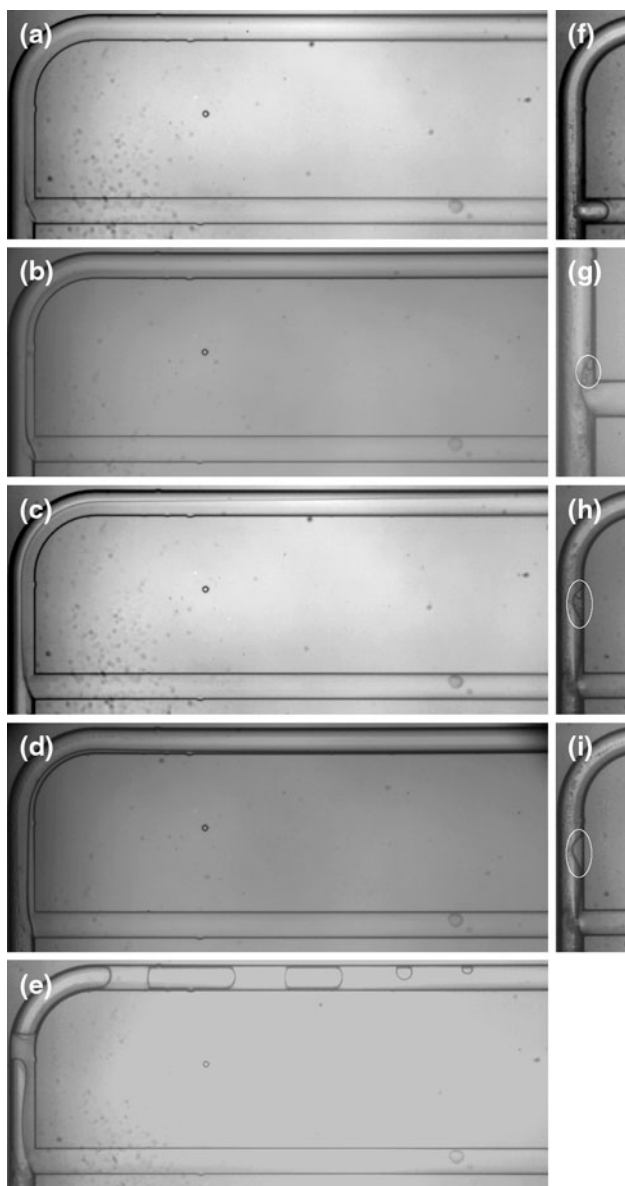


**Fig. 5** Single-phase flow, “pseudo” two-phase flow regimes and local phenomena of CO<sub>2</sub>–MeOH mixture: **a** Standard (liquid–liquid) ( $P = 13.7$  MPa,  $T = 294.0$  K); **b** Standard (supercritical–liquid) ( $P = 13.7$  MPa,  $T = 321.8$  K); **c** Stratified (smooth) ( $P = 7.87$  MPa,  $T = 308.5$  K); **d** Stratified (smooth) ( $P = 13.7$  MPa,  $T = 417.2$  K); **e** Taylor ( $P = 6.89$  MPa,  $T = 300.9$  K); **f** Meniscus ( $P = 8.84$  MPa,  $T = 474.5$  K); **g** Boiling ( $P = 10.8$  MPa,  $T = 474.5$  K); **h** Wavy-boiling ( $P = 11.8$  MPa,  $T = 474.5$  K); **i** Wavy ( $P = 12.7$  MPa,  $T = 474.5$  K). The boiling phenomena and the waves are marked for easy identification

oscillated along the alcohol channel with a frequency of a few Hertz. This is a similar phenomenon to that already studied by Ody et al. (2007), who identified a threshold pressure below which a liquid plug gets blocked at the entrance of a bifurcating T-junction. Accordingly, as the pressure increased, the meniscus turned into a liquid tip in the T-junction with a boiling phenomenon inside (Fig. 5g).

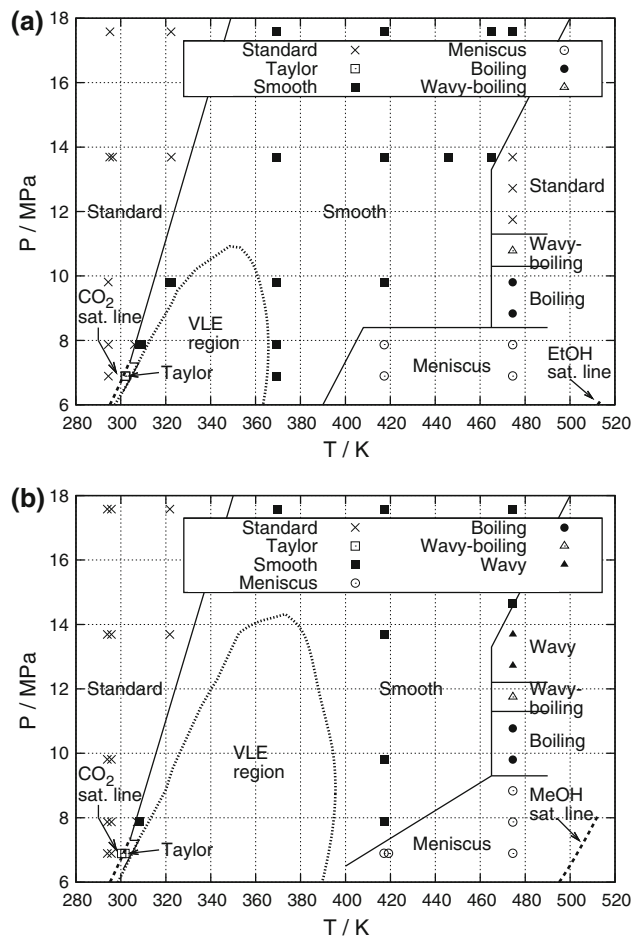


**Fig. 6** Maps of single-phase flow, “pseudo” two-phase flow regimes and local phenomena for mixtures of **a** CO<sub>2</sub>–EtOH and **b** CO<sub>2</sub>–MeOH, based on temperature and pressure conditions

By further increasing the pressure, the tip turned to “pseudo” wavy flow with boiling inside the waves (Fig. 5h) until the boiling disappeared above certain pressure (Fig. 5i).

### 3.3 Accumulation of liquid in CO<sub>2</sub> line

Dynamic instabilities are a common issue in flow of boiling fluids in microchannels, and they have been extensively reported and analysed (Thome 2006; Kandlikar 2002; Ambrosini 2007). Although none of the present experiments seemed to suffer from any of these dynamic instabilities, an unexpected phenomenon was observed during the experiments which deserves special attention. The phenomenon consisted in a continuous accumulation of liquid, either in the CO<sub>2</sub> channel before the T-junction or at the side of the channel occupied by the CO<sub>2</sub> after the T-junction. The accumulation occurred only at VLE conditions for both mixtures, starting at temperatures slightly above the bubble point until temperatures of 10–20 K

below the dew point. It was present at all pressure conditions, with the CO<sub>2</sub> in gas and supercritical state. The shadowed areas in the maps of two-phase flow regimes (Fig. 4) highlight the conditions at which this liquid accumulation was observed.

The overall process of this phenomenon can be divided into four different stages, as illustrated in the series of images of Fig. 7, corresponding to a mixture of CO<sub>2</sub>–MeOH at 6.89 MPa and 321.8 K, with a Taylor flow regime. The first stage, which could not be observed in the experiments, consists in the splitting of a small amount of liquid from the bulk flow of alcohol in the T-junction. The second stage is the displacement of the liquid upwards the CO<sub>2</sub> channel in form of tiny droplets, of sizes up to 10–15 μm, or a thin film attached to the wall. In the third stage, these droplets reach a position where they tend to coalesce and generate one or more accumulations of liquid

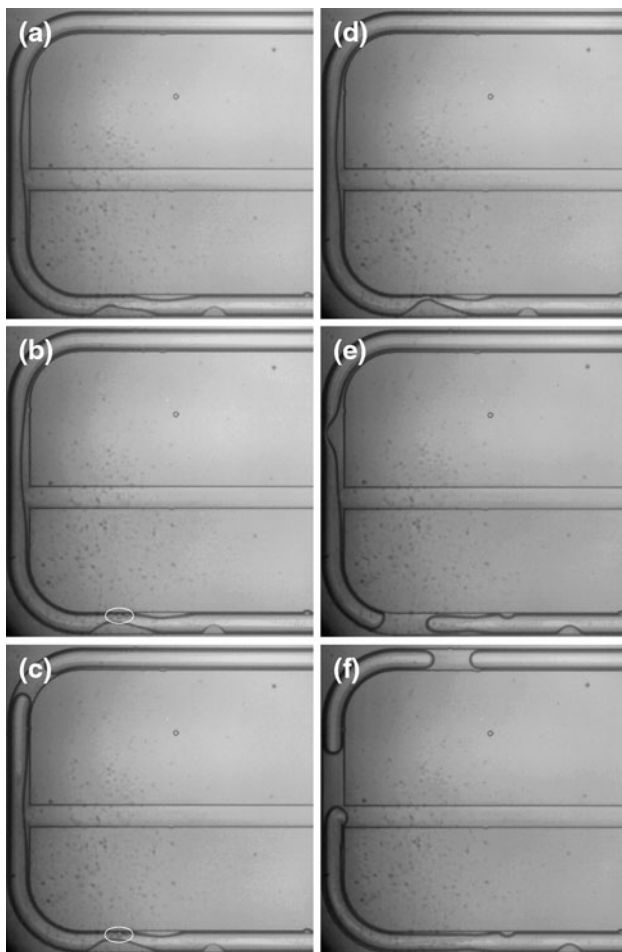


**Fig. 7** CO<sub>2</sub>–MeOH at 6.89 MPa and 321.8 K. **a–c** Evolution of the liquid accumulation in the CO<sub>2</sub> line and **d–f** further generation of a liquid plug. Elapsed time: **a** 0 ms; **b** 346.7 ms; **c** 705.3 ms; **d** 884.7 ms; **e** 892.5 ms; **f** 900.4 ms. The tiny liquid droplets coalescing with the accumulation are marked for easy identification (Video in Online Resource 2)

that increase their size with time (Fig. 7a–c). The accumulation was not always static, as it experienced a random displacement over a narrow distance along the channel, but without being dragged by the CO<sub>2</sub> stream. Finally in the fourth stage, depending on pressure and temperature conditions, the accumulation of liquid gradually grows up (Fig. 7d) until the channel gets completely blocked (Fig. 7e) and then one or more plugs of liquid are ejected downwards the channel, disturbing the whole two-phase flow regime (Fig. 7f). The blocking of the CO<sub>2</sub> channel and the subsequent formation of one or more liquid plugs occurred up to a region of 10–20 K below the high temperature limits of the phenomenon. At these high temperatures, the amount of liquid accumulated was not enough to block the channel. Finally, further above these temperatures the accumulation of liquid disappeared completely.

At higher experimental pressures (9.81 MPa) and within a narrow temperature range close to the bubble temperature (328.8–331.4 K for CO<sub>2</sub>–EtOH; 325.2–328.7 K for CO<sub>2</sub>–MeOH), the accumulation appeared first after the T-junction, at the CO<sub>2</sub> side wall of the two-phase flow. In this case, it showed a slow, periodic movement towards the T-junction as depicted in the images of Fig. 8, corresponding to a mixture of CO<sub>2</sub>–MeOH with an annular flow regime. In these images, the liquid is initially accumulated somewhere after the T-junction (Fig. 8a), then it slowly moves upwards (Fig. 8b) until it reaches a position (Fig. 8c) where it disappears while the process starts again

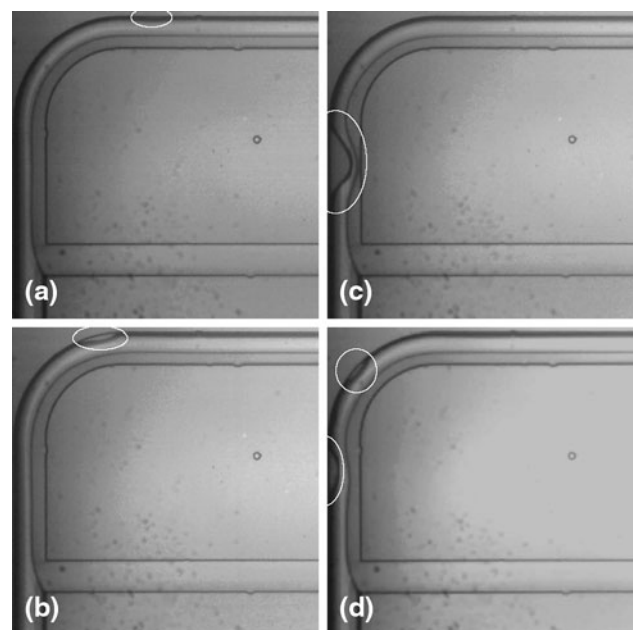


**Fig. 8** CO<sub>2</sub>–MeOH at 9.81 MPa and 325.2 K. Appearance and displacement upwards of the accumulation of liquid at the CO<sub>2</sub> side of the two-phase flow. Elapsed time: **a** 0 s; **b** 4.52 s; **c** 24.1 s; **d** 25.6 s. The accumulation is marked for easy identification (Video in Online Resource 3)



with a new accumulation appearing downwards the channel (Fig. 8d). In this way, no liquid plugs were generated. The behaviour was also different than in the previous example (Fig. 7) in the sense that no tiny liquid droplets could be observed coalescing in the accumulation. As the temperature of the system was increased several degrees, the liquid accumulation reached the position of the T-junction and surpassed it upwards, leading to the phenomenon shown in Fig. 7.

As it can be noticed from the timestamps of the images of Figs. 7 and 8, this phenomenon was a slow and random process in comparison with the usual time-scale of the two-phase flows. Compared to the average generation period of Taylor plugs in the present work, of the order of 5–200 ms, the period of the plugs from the accumulation, could be from 300 ms up to several seconds. In some occasions, a continuous bunch of liquid plugs appeared and lasted up to 0.5 s before the system stabilised and the accumulation started again. As mentioned, the time-scales and frequencies of this phenomenon showed an apparently random behaviour, thus their dependency on temperature and pressure conditions could not be properly identified. On the other hand, the experimental conditions clearly affected the average distance between the liquid accumulation and the T-junction, which increased with temperature and decreased with pressure.

This phenomenon was fully reproducible, and the continuous generation of plugs disturbed the two-phase flow regimes throughout most of the VLE conditions. Overall, it can be a drawback in the use of this kind of two-phase flow systems and, therefore, its causes should be analysed aiming for a further prevention. However, this is beyond the scope of the present study. Yet briefly, few efforts were made trying to elucidate its mechanisms. To discard the Dean effects from interactions with the curvature of the channels as a possible cause for the phenomenon, a test was performed with the inlet lines inverted, i.e. the CO<sub>2</sub> flowing through the straight side channel and the alcohols through the curved main channel. Accumulation of both alcohols before and after the T-junction could be again observed with this configuration. The result of a sudden pressure adjustment between both inlet lines in the T-junction can be also ruled out. In this case, one would expect evidences of liquid accumulation not only in VLE conditions but also during “pseudo” two-phase flows, at least at temperatures slightly below the bubble line. This, certainly, did not occur.

So far, the capillary and wetting effects due to Marangoni stresses generated by local temperature and concentration gradients in the liquid, probably are the responsible for these instabilities (Squires and Quake 2005; Kumar and Prabhu 2007). Especially, if the absorption of

CO<sub>2</sub> into the liquid alcohol in the T-junction is not instantaneously homogeneous, the temporary heterogeneous distribution of composition with concentration gradients across the liquid surface,  $\Delta x_{\text{CO}_2}$ , can lead to important gradients of several properties such as the interface tension, the density and the viscosity. These gradients might generate Marangoni stresses sufficient to induce the splitting of small amounts of liquid from the bulk flow (the first stage of the phenomenon, previously identified) and their displacement upwards the channel (second stage). This displacement stops once the liquid droplets reach equilibrium composition and they coalesce (third stage). Then, the prevailing surface tension forces of the liquid over the viscous/inertial forces of the CO<sub>2</sub> stream (Capillary and Weber numbers) ensure that the liquid accumulation is not dragged by the CO<sub>2</sub> stream. Finally, the continuous stream of pure CO<sub>2</sub> flowing over the isolated liquid causes a continuous transport of alcohol from the accumulation to the stream. As a result of the balance between the liquid coalescing and the liquid being transported to the stream, either the channel ends up clogged by the liquid (fourth stage), as in Fig. 7, or the accumulation reduces its size and eventually disappears, as in Fig. 8 and at the higher temperatures. It is important to note that the characteristic semicircular cross section of the channels enhances the role of the surface tension and supports the phenomenon, due to the increased contact surface between the liquid and the channel, and to the decreased flow velocities near the corners of the channel.

### 3.4 Two-phase void fraction

The void fraction of a two-phase flow,  $\varepsilon_{\text{exp}}$ , represents the fraction of volume within the channel occupied by the gas phase and, when compared to the homogeneous void fraction,  $\varepsilon_{\text{hom}}$ , it gives information on the slip between the average velocities of the gas and the liquid phases.  $\varepsilon_{\text{hom}}$  is the ratio of gas volumetric flow rate to total volumetric flow rate, and it can be understood as the resulting void fraction in VLE conditions if both phases would flow with the same average velocities. In this case  $\varepsilon_{\text{exp}}$  equals  $\varepsilon_{\text{hom}}$ .

$\varepsilon_{\text{exp}}$  in the microchannel after the T-junction was obtained as described in Sect. 2.4.  $\varepsilon_{\text{hom}}$  was calculated as a function of the vaporised mass diffusion fraction,  $G_d$ , and of the densities of the vapour and the liquid phases,  $\rho_v$  and  $\rho_l$ , (Revellin 2005),

$$\varepsilon_{\text{hom}} = \frac{1}{1 + (1/G_d - 1)\rho_v/\rho_l} \quad (5)$$

In binary systems,  $G_d$  is the analogous to the vapour quality of single boiling fluids (Collier and Thome 1996), and is defined as,

$$G_d = \frac{x_{0,\text{CO}_2} - x_{\text{CO}_2}}{y_{\text{CO}_2} - x_{\text{CO}_2}} \quad (6)$$

Pure CO<sub>2</sub> was assumed when calculating  $\rho_v$ , according to the high content of CO<sub>2</sub> in vapour phase throughout all VLE conditions.

The void fractions are plotted against the relative temperature,  $T_{\text{rel}}$ , in Fig. 9 for both sets of fluids at the three different pressures.  $T_{\text{rel}}$  is a normalised dimensionless temperature that relates the actual temperature to the bubble and dew temperatures. It is defined as,

$$T_{\text{rel}} = \frac{T - T_{\text{bub}}}{T_{\text{dew}} - T_{\text{bub}}} \quad (7)$$

In this work, plotting the void fractions against the relative temperature instead of against the usual homogeneous void fraction (Kawahara et al. 2002; Serizawa et al. 2002; Yue et al. 2008; de Loos et al. 2010) or vapour quality (Revellin et al. 2006; Agostini et al. 2008) allowed a clearer analysis of the results.

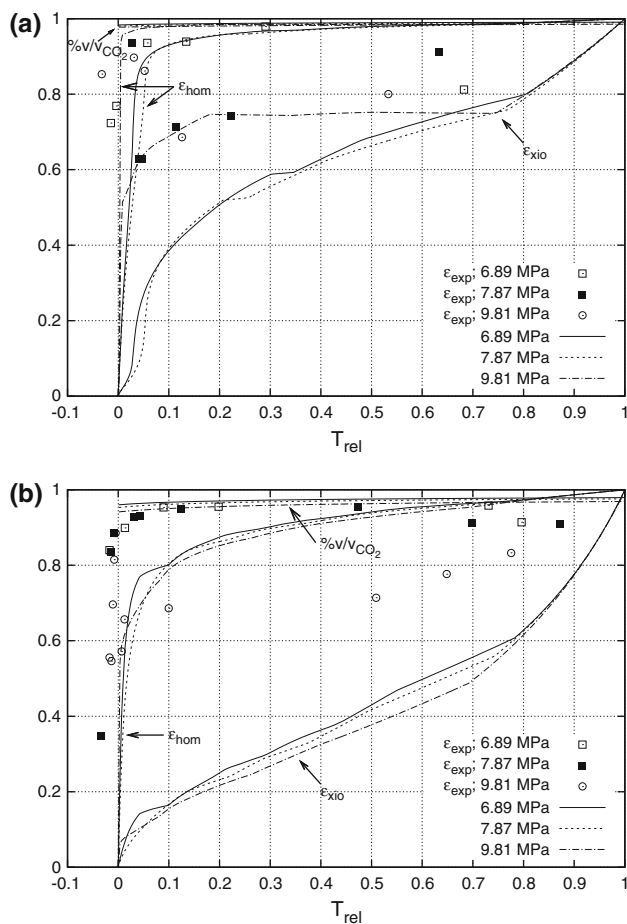


**Fig. 9** Comparison of experimental void fraction,  $\varepsilon_{\text{exp}}$ , homogeneous void fraction,  $\varepsilon_{\text{hom}}$ , and the correlation of Xiong and Chung (2007),  $\varepsilon_{\text{xio}}$  against the relative temperature, at 6.89, 7.87 and 9.81 MPa. **a** CO<sub>2</sub>-EtOH at  $x_{0,\text{CO}_2} = 0.95$  ( $\%v/v_{\text{CO}_2} \approx 0.977$  to 0.991) and **b** CO<sub>2</sub>-MeOH at  $x_{0,\text{CO}_2} = 0.87$  ( $\%v/v_{\text{CO}_2} \approx 0.941$  to 0.979)

A sharp variation of  $\varepsilon_{\text{hom}}$  in a very narrow range of temperatures above the bubble point,  $T_{\text{rel}} < 0.1$ , can be observed in Fig. 9 for both sets of fluids and all pressures. This is the result of the sudden decrease in mass fraction of CO<sub>2</sub> in the liquid phase close to the bubble point (Fig. 2). As a consequence, the system becomes extremely sensitive to temperature changes within a range of 3–5 K above the bubble point, affecting the two-phase flows transitions (Fig. 4) and the dynamics of Taylor flow (see Sect. 3.5) in this region.

When analysing the results of  $\varepsilon_{\text{exp}}$ , two tendencies can be noticed depending on the flow regime of the experiment. On one hand, Taylor flow (6.89 MPa series in Fig. 9a, and 6.89 and 7.87 MPa series in Fig. 9b) quickly reaches high values,  $\varepsilon_{\text{exp}} > 0.9$ , exceeding those of  $\varepsilon_{\text{hom}}$ , and then it stabilises as  $T_{\text{rel}}$  increases. On the other hand, wavy and annular flows (7.87 and 9.81 MPa series in Fig. 9a, and 9.81 MPa series in Fig. 9b), after a region of unstable results near the bubble point, show moderate values, below  $\varepsilon_{\text{hom}}$ , with a gradual increment with  $T_{\text{rel}}$ . These two trends agree with the idea that, unlike Taylor flow where vapour is surrounded by liquid plugs, in stratified flows such as annular and wavy the vapour phase can flow unhindered and, therefore, slip between both velocities is likely to occur, resulting in lower  $\varepsilon_{\text{exp}}$  values.

The volumetric fraction of CO<sub>2</sub>,  $\%v/v_{\text{CO}_2}$ , corresponding to the initial volumetric ratio at which both fluids reach the T-junction, was calculated with the aim to clarify those cases when  $\varepsilon_{\text{exp}}$  exceeds  $\varepsilon_{\text{hom}}$ .  $\%v/v_{\text{CO}_2}$  was obtained similarly to  $\varepsilon_{\text{hom}}$  (Eq. 5),

$$\%v/v_{\text{CO}_2} = \frac{1}{1 + (1/x_{0,\text{CO}_2} - 1)\rho_{\text{CO}_2}/\rho} \quad (8)$$

Here,  $\rho$  is the density of the pure alcohol in the T-junction.

It can be observed in Fig. 9 that  $\%v/v_{\text{CO}_2}$  is similar to  $\varepsilon_{\text{exp}}$  of Taylor flows, suggesting the possibility that, in these cases, the flow does not reach complete VLE conditions inside the visualised area, in particular at low temperatures where the difference between  $\%v/v_{\text{CO}_2}$  and the void fraction at VLE conditions,  $\varepsilon_{\text{hom}}$ , is larger. On the other hand, the evolution towards VLE conditions in stratified flows is faster than in Taylor flows, as demonstrated by the lower  $\varepsilon_{\text{exp}}$  obtained in these flow regimes.

The similar behaviour of VLE at all pressures, together with moderate differences between  $\rho_l$  and  $\rho_v$ , resulted in a negligible effect of pressure on the distribution of  $\varepsilon_{\text{hom}}$ . Furthermore, this can be corroborated with the similar results of  $\varepsilon_{\text{exp}}$  at different pressures for the same flow regime.

$\varepsilon_{\text{exp}}$  is compared with the void fraction predicted with the correlation of Xiong and Chung (2007),  $\varepsilon_{\text{xio}}$ , in Fig. 9. This correlation (Eqs. 9 and 10) has been tested in adiabatic

systems with square, rectangular and circular microchannels of  $d_h \leq 1$  mm. It was developed accounting for different flow regimes, including Taylor, annular and wavy flows.

$$\varepsilon_{xio} = \frac{C \cdot \varepsilon_{hom}^{0.5}}{1 - (1 - C) \cdot \varepsilon_{hom}^{0.5}} \tag{9}$$

$$C = \frac{0.266}{1 + 13.8 \cdot \exp(-0.00688 d_h)} \tag{10}$$

It can be observed in Fig. 9 that  $\varepsilon_{xio}$  underestimates  $\varepsilon_{exp}$ , especially for Taylor flows. However, the qualitative trend of  $\varepsilon_{xio}$  with  $T_{rel}$  is in agreement with the  $\varepsilon_{exp}$  of annular flows.

A considerable amount of studies of adiabatic Taylor-like flows (de Loos et al. 2010; Serizawa et al. 2002; Yue et al. 2008) have reported linear relationships of  $\varepsilon_{exp}$  with  $\varepsilon_{hom}$ , in agreement with Armand-like correlations (Armand 1946; Ali et al. 1993). To some extent, the present results in Taylor flow might as well indicate a linear relationship between both void fractions, despite the higher  $\varepsilon_{exp}$  than  $\varepsilon_{hom}$ .

### 3.5 Dynamics of Taylor flow

Segmented flows, including Taylor flow, are among the most interesting flow regimes in multiphase microscale engineering, due to their broad range of applications and to their already identified advantages (Shui et al. 2007b; Günther and Jensen 2006). Furthermore, their mechanisms of formation are more complex than those of stratified regimes, and they have been extensively studied (e.g. Guillot and Colin 2005; Gupta and Kumar 2009; Liu and Zhang 2009; Marre et al. 2009; Lee et al. 2008). Altogether, their characterisation and the identification of their hydrodynamics become challenging tasks of great interest.

Taylor flow has been characterised in the present study, and the resulting elongation rates, frequencies of generation of liquid plugs and jet entrainments are presented here against  $T_{rel}$  (Eq. 7), for both sets of fluids at the different operating pressures.

Together with a continuous decrease of the average velocity of bubbles, a variation in the length of liquid plugs as they travelled along the channel was observed. This length variation was measured in the form of a dimensionless elongation rate,  $\theta$ , given in Eq. 3 and plotted in Fig. 10. It can be seen that all series of experiments experience an initial sharp decrease near the bubble temperature and reach minima at  $T_{rel} \approx 0.1-0.2$ . Then, there is an increase up to values around 0.1.

The length of bubbles depends mainly on the phenomena occurring in the region where both fluids meet, due to the predominance of surface tension (Hessel et al. 2005;

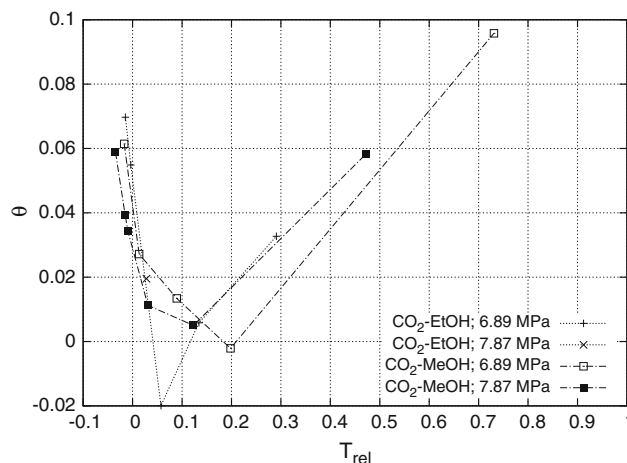


**Fig. 10** Rate of elongation,  $\theta$ , of liquid plugs of Taylor flow for CO<sub>2</sub>–EtOH and CO<sub>2</sub>–MeOH at 6.89 and 7.87 MPa, against the relative temperature

van Steijn et al. 2007). Accordingly, given the positive values of  $\theta$ , the coalescence of bubbles and the bubble-train flow, previously reported in adiabatic (Dreyfus et al. 2003; Yue et al. 2008) and non-adiabatic (Revellin et al. 2006, 2008) studies, are not expected to occur here downwards the channel.

The elongation of liquid plugs can be explained by two mechanisms. The difference between the volumetric fraction when both fluids join in the T-junction and the void fraction at VLE conditions is especially large at low temperatures (Fig. 9). Thus, in that region the prevalent mechanism is the progressive absorption of CO<sub>2</sub> into the liquid phase along the channel to reach VLE compositions. The gap between  $\%v/v_{CO_2}$  and  $\varepsilon_{hom}$  decreases sharply as temperature increases, so does the absorption of CO<sub>2</sub> and the elongation of liquid plugs. This trend is reverted at  $T_{rel} > 0.1-0.2$  when the previous decrease in absorption of CO<sub>2</sub> is offset by a second mechanism related to the frequency of generation of liquid plugs,  $f_{lp}$ . Figure 11 shows how  $f_{lp}$  experiences a sharp decrease as  $T_{rel}$  increases in all series of experiments, with an inflection point in the system behaviour at  $T_{rel} \approx 0.1-0.2$ , from larger to smoother gradients of  $f_{lp}$ . Above that inflection point  $f_{lp}$  is small, and there is time enough after a plug for a liquid layer to build up along the channel wall. When the next liquid plug is generated, it gathers the liquid in the layer as it passes through, progressively increasing its length.

The dimensionless jet entrainment, defined as the distance between the T-junction and the position where the liquid plugs were generated, scaled with the hydraulic diameter of the channel, is shown in Fig. 12. Very large values of jet entrainment and high dependency of temperature are typical at temperatures close to the bubble point, reaching an inflection point at  $T_{rel} \approx 0.1-0.2$  with

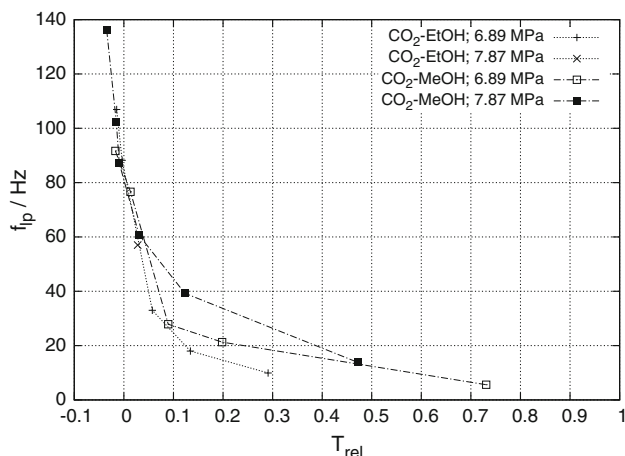


**Fig. 11** Frequency of generation,  $f_p$ , of liquid plugs of Taylor flow for  $\text{CO}_2$ -EtOH and  $\text{CO}_2$ -MeOH at 6.89 and 7.87 MPa, against the relative temperature

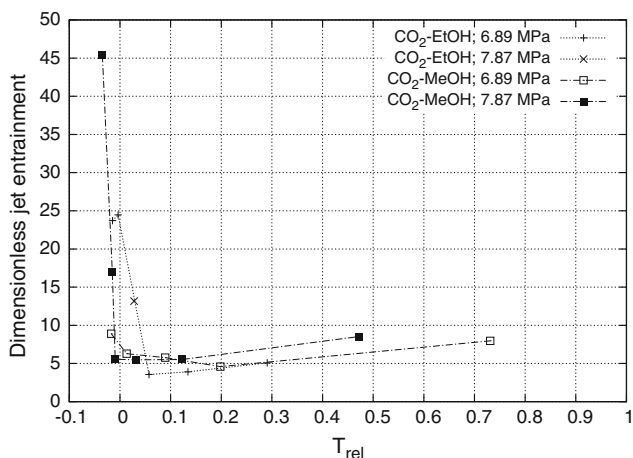


**Fig. 12** Dimensionless jet entrainment of Taylor flow for  $\text{CO}_2$ -EtOH and  $\text{CO}_2$ -MeOH at 6.89 and 7.87 MPa, against the relative temperature

minimum values of  $\approx 5$ . The jet entrainment is then stabilised, with slightly positive gradients with  $T_{\text{rel}}$ . According to the definitions of de Menech et al. (2008) and Steegmans et al. (2009), and to the long jet entrainments obtained, most of the present Taylor flows would clearly show a jetting regime of formation of bubbles, thus denoting relative importance of viscous and inertial forces.

Overall, from the present analysis, the temperature and, by extension, the vaporisation conditions of the system (see Sect. 3.4), can be identified as the main agents affecting the hydrodynamics of Taylor flows, with a common inflection point in the behaviour of most of the results at  $T_{\text{rel}} \approx 0.1$ – $0.2$ . On the other hand, both sets of fluids showed very similar hydrodynamics, which is coherent with the resemblance in the phase behaviour of both mixtures, and in the physical and transport properties of both liquid

phases. Finally, the effect of pressure was mostly negligible, and no differences were observed when using  $\text{CO}_2$  in gas or supercritical state.

## 4 Conclusions

The present work analysed the single- and two-phase flow behaviour in microchannels of two binary mixtures,  $\text{CO}_2$ -ethanol and  $\text{CO}_2$ -methanol, with the  $\text{CO}_2$  in liquid, gas or supercritical state. These were experimentally investigated in a non-adiabatic microfluidic T-junction with a semicircular cross section. Under the considered conditions of pressure, temperature and mass fraction of  $\text{CO}_2$ , the mixtures were either in miscible single phase, or in VLE with two immiscible separated phases composed, each, by both fluids.

Taylor, annular and wavy were the two-phase flow regimes observed, with predominance of annular flow at higher pressures and temperatures, and of Taylor flow at lower pressures and temperatures. Taylor flows showed a jetting regime of generation, given their large dimensionless jet entrainments. Also, a sharp decrease in their frequency of plug generation with relative temperature resulted in extremely long gas bubbles at the higher temperatures.

In single phase, the flows were classified into three different groups: standard single-phase flows, “pseudo” two-phase flows and local phenomena in the T-junction. Taylor, stratified (smooth) and wavy were the observed “pseudo” two-phase flows, with predominance of stratified flow. The local phenomena were only present at high temperatures, and consisted of a liquid meniscus and boiling.

A dynamic phenomenon was found in VLE conditions, consisting of a continuous accumulation of liquid either in the  $\text{CO}_2$  channel before the T-junction or at the  $\text{CO}_2$ -side wall after the T-junction. The liquid accumulation periodically blocked the channel and was followed by ejection of several liquid plugs downwards, causing a transient instability that disturbed the whole flow. The capillary and wetting effects due to Marangoni stresses generated by local temperature and concentration gradients in the liquid were suggested as the most probable causes of the phenomenon.

From the study of two-phase void fractions, extremely high vaporisation values were observed throughout most of the operating conditions, starting around 3–5 K above the bubble point temperature. The excess of experimental to homogeneous void fraction values with Taylor flows, suggested the possibility that the flow did not reach thermodynamic equilibrium in the visualised area in these cases. However, the qualitative trend of the experimental



void fractions agreed with Armand-like correlations in the case of Taylor flow, and with the correlation of Xiong and Chung (2007) in the case of annular and wavy flows.

Overall, the two-phase flows obtained in the present work with the CO<sub>2</sub> in supercritical state and with the mixtures in VLE conditions do not differ morphologically to those two-phase flows in microchannels, already reported in the literature, formed by single boiling fluids or by immiscible fluids in adiabatic conditions without mass transport between phases. From the analysis of the two-phase void fractions and the hydrodynamics of Taylor flows, it can be concluded that pressure and CO<sub>2</sub> state played a minor role in the results. Also, both sets of fluids experienced very similar results, mostly due to the high content of CO<sub>2</sub> in the liquid phase as well as in the gas phase. On the other hand, temperature was a determinant in the system, and most of the series of results based on relative temperature showed qualitative and quantitative agreement.

**Acknowledgments** The authors are grateful to Professor John R. Thome of the EPFL, Lausanne, Switzerland, for the valuable discussions. This study was financially supported by the Spanish Ministry of Science and Technology and FEDER under project DPI2010-17212. R. B. acknowledges the financial support by the Spanish Ministry of Education through the mobility grants programme for PhD students.

## References

- Agostini B, Revellin R, Thome JR (2008) Elongated bubbles in microchannels. Part I: Experimental study and modeling of elongated bubble velocity. *Int J Multiph Flow* 34(6):590–601
- Akbar MK, Plummer DA, Ghiaasiaan SM (2003) On gas–liquid two-phase flow regimes in microchannels. *Int J Multiph Flow* 29(5):855–865
- Ali MI, Sadatomi M, Kawaji M (1993) Adiabatic two-phase flow in narrow channels between two flat plates. *Can J Chem Eng* 71(5):657–666
- Ambrosini W (2007) On the analogies in the dynamic behaviour of heated channels with boiling and supercritical fluids. *Nucl Eng Des* 237(11):1164–1174
- Armand AA (1946) The resistance during the movement of a two-phase system in horizontal pipes. *Izv Vses Teplotekh Inst* 1:16–23 (A.E.R.E. Lib/Trans 828)
- Bezanehtak K, Combes GB, Dehghani F, Foster NR, Tomasko DL (2002) Vapor–liquid equilibrium for binary systems of carbon dioxide + methanol, hydrogen + methanol, and hydrogen + carbon dioxide at high pressures. *J Chem Eng Data* 47(2):161–168
- Brunner E, Hültenschmidt W, Schlichthärle G (1987) Fluid mixtures at high pressures IV. Isothermal phase equilibria in binary mixtures consisting of (methanol + hydrogen or nitrogen or methane or carbon monoxide or carbon dioxide). *J Chem Thermodyn* 19(3):273–291
- Chehroudi B (2006) Supercritical fluids: nanotechnology and select emerging applications. *Combust Sci Technol* 178(1):555–621
- Cheng L, Ribatski G, Thome JR (2008) Analysis of supercritical CO<sub>2</sub> cooling in macro- and micro-channels. *Int J Refrig* 31(8):1301–1316
- Chester TL (2004) Determination of pressure-temperature coordinates of liquid–vapor critical loci by supercritical fluid flow injection analysis. *J Chromatogr A* 1037(1–2):393–403
- Chung PMY, Kawaji M (2004) The effect of channel diameter on adiabatic two-phase flow characteristics in microchannels. *Int J Multiph Flow* 30(7–8):735–761
- Collier JG, Thome JR (1996) *Convective Boiling and Condensation*, 3rd edn. Oxford University Press, USA
- Dang C, Iino K, Hihara E (2008) Study on two-phase flow pattern of supercritical carbon dioxide with entrained PAG-type lubricating oil in a gas cooler. *Int J Refrig* 31(7):1265–1272
- Dreyfus R, Tabeling P, Willaime H (2003) Ordered and disordered patterns in two-phase flows in microchannels. *Phys Rev Lett* 90(14):144505
- Galicia-Luna LA, Ortega-Rodriguez A, Richon D (2000) New apparatus for the fast determination of high-pressure vapor–liquid equilibria of mixtures and of accurate critical pressures. *J Chem Eng Data* 45(2):265–271
- Garstecki P, Fuerstman MJ, Stone HA, Whitesides GM (2006) Formation of droplets and bubbles in a microfluidic T-junction—scaling and mechanism of break-up. *Lab Chip* 6(3):437–446
- Guido S, Preziosi V (2010) Droplet deformation under confined Poiseuille flow. *Adv Colloid Interface Sci* 161(1–2):89–101
- Guillot P, Colin A (2005) Stability of parallel flows in a microchannel after a T junction. *Phys Rev E Stat Nonlinear Soft Matter Phys* 72(6):066301
- Günther A, Jensen KF (2006) Multiphase microfluidics: from flow characteristics to chemical and materials synthesis. *Lab Chip* 6(12):1487–1503
- Gupta A, Kumar R (2009) Effect of geometry on droplet formation in the squeezing regime in a microfluidic T-junction. *Microfluid Nanofluid* 8(6):799–812
- Hessel V, Angeli P, Gavriilidis A, Löwe H (2005) Gas–liquid and gas–liquid–solid microstructured reactors: Contacting principles and applications. *Ind Eng Chem Res* 44(25):9750–9769
- Hwang JJ, Tseng FG, Pan C (2005) Ethanol–CO<sub>2</sub> two-phase flow in diverging and converging microchannels. *Int J Multiph Flow* 31(5):548–570
- Jennings DW, Lee RJ, Teja AS (1991) Vapor–liquid equilibria in the carbon dioxide + ethanol and carbon dioxide + 1-butanol systems. *J Chem Eng Data* 36(3):303–307
- Joung SN, Yoo CW, Shin HY, Kim SY, Yoo KP, Lee CS, Huh WS (2001) Measurements and correlation of high-pressure VLE of binary CO<sub>2</sub>–alcohol systems (methanol, ethanol, 2-methoxyethanol and 2-ethoxyethanol). *Fluid Phase Equilibria* 185(1–2):219–230
- Kandlikar SG (2002) Fundamental issues related to flow boiling in minichannels and microchannels. *Exp Thermal Fluid Sci* 26(2–4):389–407
- Kawahara A, Chung PMY, Kawaji M (2002) Investigation of two-phase flow pattern, void fraction and pressure drop in a microchannel. *Int J Multiph Flow* 28(9):1411–1435
- Kumar G, Prabhu KN (2007) Review of non-reactive and reactive wetting of liquids on surfaces. *Adv Colloid Interface Sci* 133(2):61–89
- Lee CY, Lee SY (2008) Influence of surface wettability on transition of two-phase flow pattern in round mini-channels. *Int J Multiph Flow* 34(7):706–711
- Lee LY, Lim LK, Hua J, Wang CH (2008) Jet breakup and droplet formation in near-critical regime of carbon dioxide-dichloromethane system. *Chem Eng Sci* 63(13):3366–3378
- Leu AD, Chung SYK, Robinson DB (1991) The equilibrium phase properties of (carbon dioxide + methanol). *J Chem Thermodyn* 23(10):979–985

- Liu H, Zhang Y (2009) Droplet formation in a T-shaped microfluidic junction. *J Appl Phys* 106(3):034906
- de Loos SRA, van der Schaaf J, Tiggelaar RM, Nijhuis TA, de Croon MHJM, Schouten JC (2010) Gas–liquid dynamics at low Reynolds numbers in pillared rectangular micro channels. *Microfluidics and Nanofluidics* 9(1):131–144
- Marre S, Aymonier C, Subra P, Mignard E (2009) Dripping to jetting transitions observed from supercritical fluid in liquid microflows. *Appl Phys Lett* 95(13):134105
- Mendoza de la Cruz JL, Galicia-Luna LA (1999) High-pressure vapor–liquid equilibria for the carbon dioxide + ethanol and carbon dioxide + propan-1-ol systems at temperatures from 322.36 K to 391.96 K. *ELDATA Int Electr J Physico-Chem Data* 5:157–164
- de Menech M, Garstecki P, Jousse F, Stone HA (2008) Transition from squeezing to dripping in a microfluidic T-shaped junction. *J Fluid Mech* 595:141–161
- Ody CP, Baroud CN, de Langre E (2007) Transport of wetting liquid plugs in bifurcating microfluidic channels. *J Colloid Interface Sci* 308(1):231–238
- Ohgaki K, Katayama T (1976) Isothermal vapor–liquid equilibrium data for binary systems containing carbon dioxide at high pressures: methanol-carbon dioxide, n-hexane-carbon dioxide, and benzene-carbon dioxide systems. *J Chem Eng Data* 21(1):53–55
- Rasband WS (1997–2011) ImageJ, Version 1.43i. <http://rsb.info.nih.gov/ij/>
- Revellin R (2005) Experimental two-phase fluid flow in microchannels. PhD thesis, EPFL, Lausanne, Switzerland
- Revellin R, Dupont V, Ursenbacher T, Thome JR, Zun I (2006) Characterization of diabatic two-phase flows in microchannels: flow parameter results for R-134a in a 0.5 mm channel. *Int J Multiph Flow* 32(7):755–774
- Revellin R, Agostini B, Thome JR (2008) Elongated bubbles in microchannels. Part II: Experimental study and modeling of bubble collisions. *Int J Multiph Flow* 34(6):602–613
- Secuianu C, Ferioiu V, Geană D (2008) Phase behavior for carbon dioxide + ethanol system: Experimental measurements and modeling with a cubic equation of state. *J Supercrit Fluids* 47(2):109–116
- Serizawa A, Feng Z, Kawara Z (2002) Two-phase flow in microchannels. *Exp Thermal Fluid Sci* 26(6–7):703–714
- Shao N, Gavriilidis A, Angeli P (2009) Flow regimes for adiabatic gas–liquid flow in microchannels. *Chem Eng Sci* 64(11):2749–2761
- Shui L, Eijkel JCT, van den Berg A (2007a) Multiphase flow in micro- and nanochannels. *Sens Actuators B Chem* 121(1):263–276
- Shui L, Eijkel JCT, van den Berg A (2007b) Multiphase flow in microfluidic systems—Control and applications of droplets and interfaces. *Adv Colloid Interface Sci* 133(1):35–49
- Smith JM, Van Ness HC, Abbott MM (2000) Introduction to chemical engineering thermodynamics, chap 10, 6th edn. McGraw-Hill Education (ISE Editions), New York
- Squires TM, Quake SR (2005) Microfluidics: fluid physics at the nanoliter scale. *Rev Modern Phys* 77(3):977–1026
- Steegmans MLJ, Schroën CGPH, Boom RM (2009) Generalised insights in droplet formation at T-junctions through statistical analysis. *Chem Eng Sci* 64(13):3042–3050
- van Steijn V, Kreutzer MT, Kleijn CR (2007)  $\mu$ -PIV study of the formation of segmented flow in microfluidic T-junctions. *Chem Eng Sci* 62(24):7505–7514
- Suzuki K, Sue H, Itou M, Smith RL, Inomata H, Arai K, Saito S (1990) Isothermal vapor–liquid equilibrium data for binary systems at high pressures: carbon dioxide-methanol, carbon dioxide-ethanol, carbon dioxide-1-propanol, methane-ethanol, methane-1-propanol, ethane-ethanol, and ethane-1-propanol systems. *J Chem Eng Data* 35(1):63–66
- Thome JR (2006) State-of-the-art overview of boiling and two-phase flows in microchannels. *Heat Transf Eng* 27(9):4–19
- Tian YL, Han M, Chen L, Feng JJ, Qin Y (2001) Study on vapor–liquid phase equilibria for CO<sub>2</sub> – C<sub>2</sub>H<sub>5</sub>OH system. *Acta Physico Chimica Sinica* 17(2):155–160 (in Chinese)
- Tiggelaar RM, Benito-López F, Hermes DC, Rathgen H, Egberink RJM, Mugele FG, Reinhoudt DN, van den Berg A, Verboom W, Gardeniers HJGE (2007) Fabrication, mechanical testing and application of high-pressure glass microreactor chips. *Chem Eng J* 131(1–3):163–170
- Trachsel F, Tidona B, Desportes S, von Rohr PR (2009) Solid catalyzed hydrogenation in a Si/glass microreactor using supercritical CO<sub>2</sub> as the reaction solvent. *J Supercrit Fluids* 48(2):146–153
- Weinmueller C, Hotz N, Mueller A, Poulikakos D (2009) On two-phase flow patterns and transition criteria in aqueous methanol and CO<sub>2</sub> mixtures in adiabatic, rectangular microchannels. *Int J Multiph Flow* 35(8):760–772
- Xiong R, Chung JN (2007) An experimental study of the size effect on adiabatic gas–liquid two-phase flow patterns and void fraction in microchannels. *Phys Fluids* 19(3):033301
- Yue J, Luo L, Gonthier Y, Chen G, Yuan Q (2008) An experimental investigation of gas–liquid two-phase flow in single microchannel contactors. *Chem Eng Sci* 63(16):4189–4202